Supporting Information

Mechanistic Insights into the Electrochemical Reduction of CO_2 to CO on Nanostructured Ag Surfaces

Jonathan Rosen,[1,†] Gregory S. Hutchings,[1,†] Qi Lu,[1] Sean Rivera,[1] Yang Zhou,[2] Dionisios G. Vlachos,[1] and Feng Jiao,[1,*]

[1] Center for Catalytic Science and Technology (CCST), Department of Chemical and Biomolecular Engineering, University of Delaware, 150 Academy Street, Newark, DE 19716 (USA).
[2] Department of Physics and Astronomy, University of Delaware, Newark, DE 19716 (USA).

*To whom correspondence should be addressed. E-mail: jiao@udel.edu.

†These authors contribute equally to this work.

Table of Contents

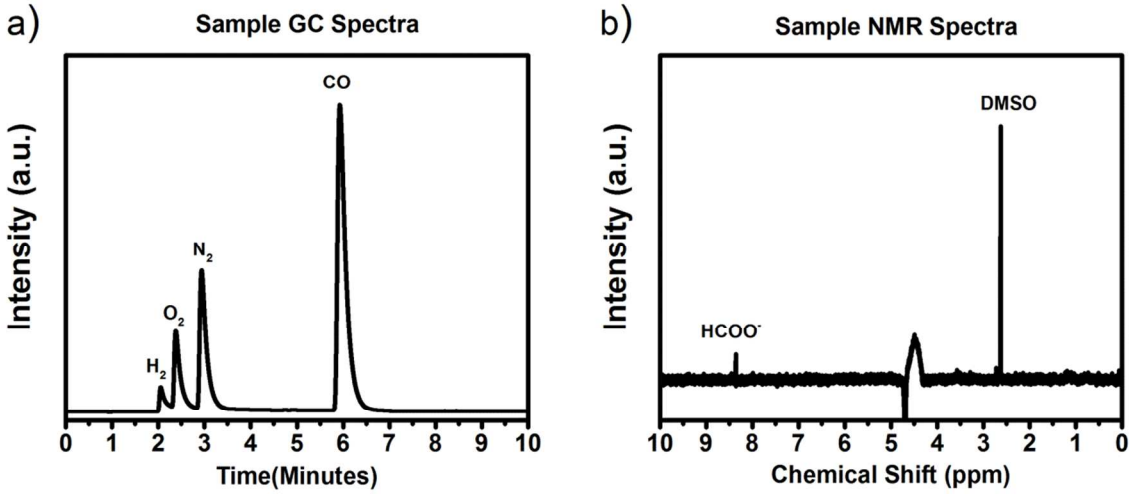

Figure S1: Sample GC and NMR Spectra. The negative intensity for H_2 peak in (a) was caused by the saturation of PDHID detector. The oxygen and nitrogen peaks were from air contamination. The peak at a chemical shift of ~4.6ppm in (b) is due to the water peak removal.

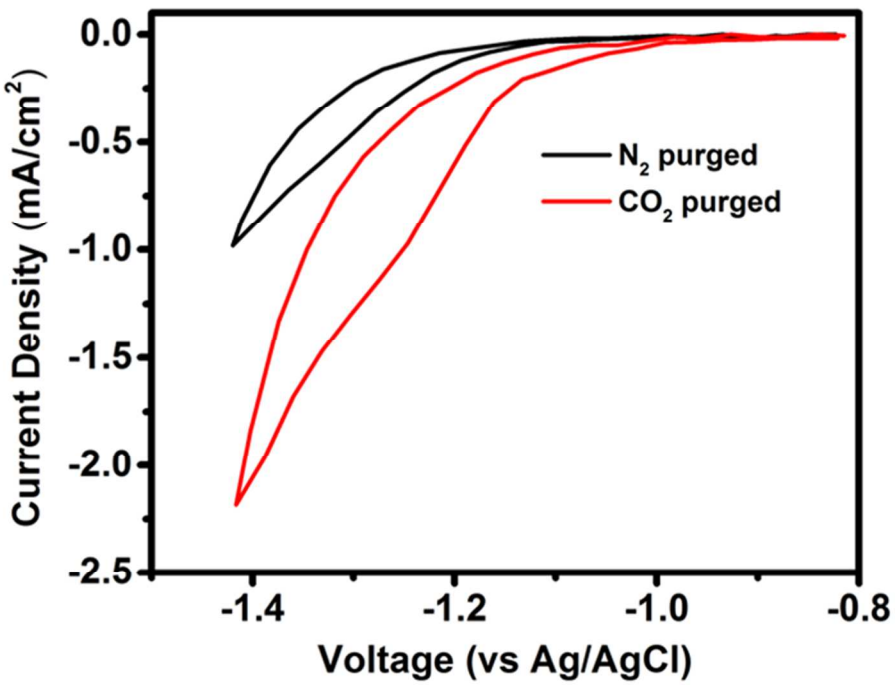

Figure S2: Cyclic voltammetry of bulk Ag electrolyte in 0.5M $NaHCO_3$ aqueous electrolyte.

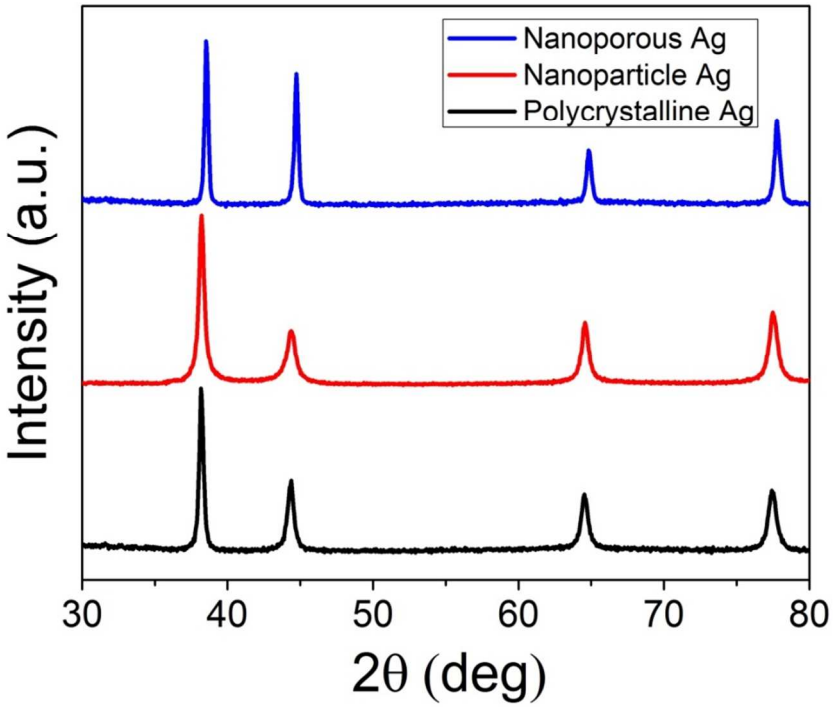

Figure S3: High-angle PXRD patterns of as prepared nanoporous Ag, nanoparticle Ag, and Ag foil.

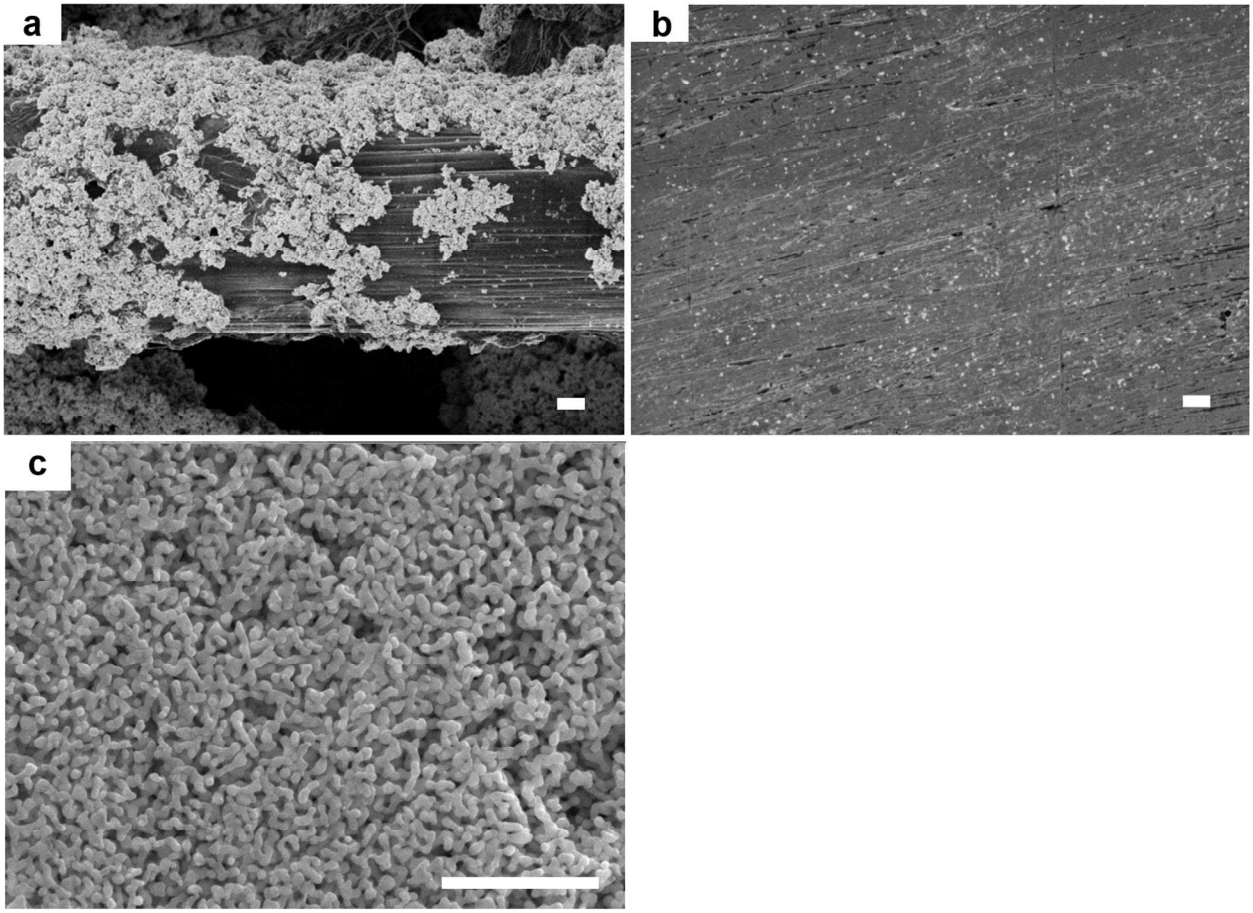

Figure S4: SEM images of Ag electrodes: (a) nanoparticle (10mg/cm^2 loading), (b) bulk, and (c) nanoporous silver (scale bar 1 μm).

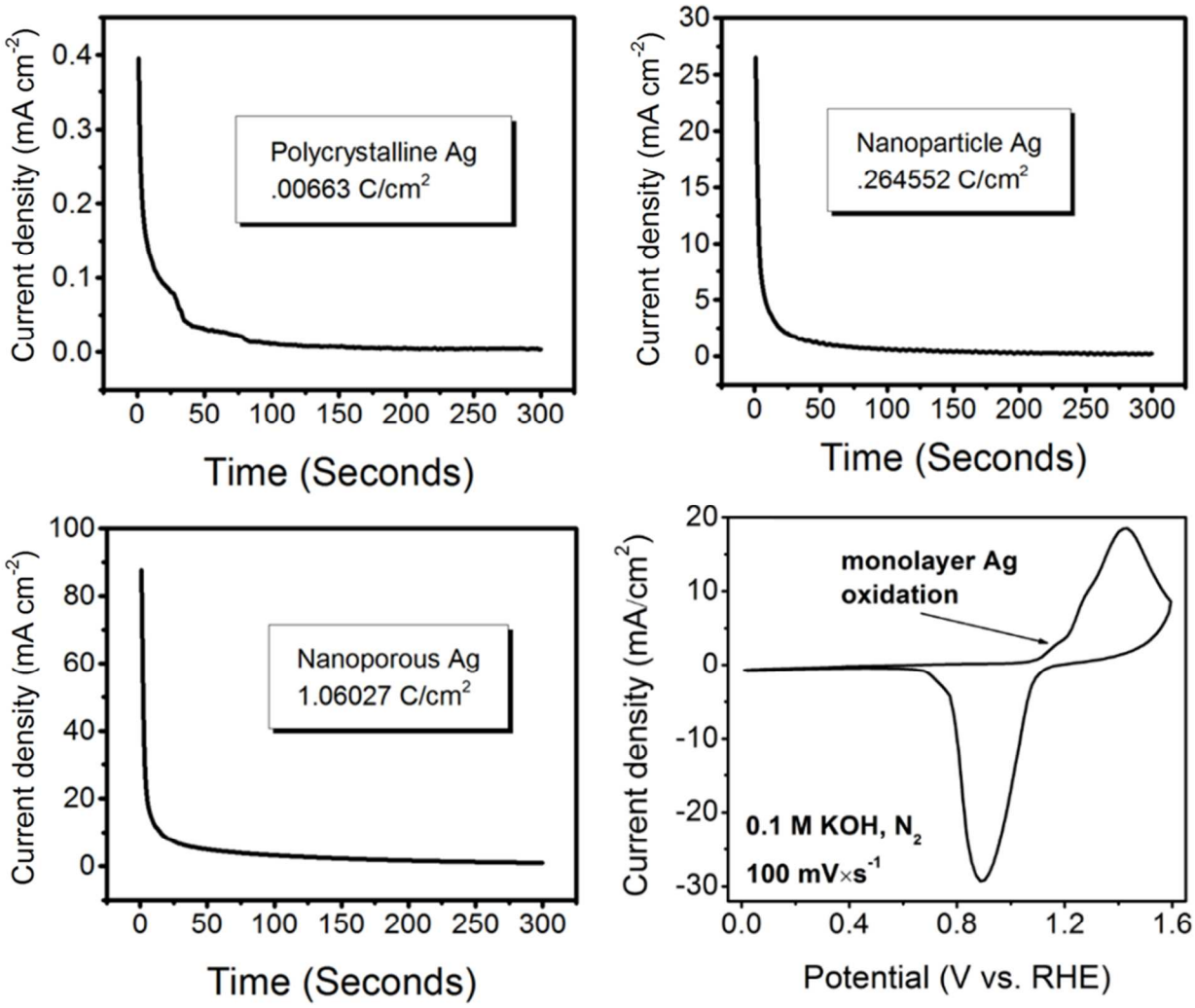

Figure S5. Electrochemical active surface areas of Ag catalysts using the monolayer oxide method. A typical cyclic voltammogram of Ag within the potential widow of 0 to 1.60 V vs. RHE is presented. The current peak observed at about 1.15 V corresponds to a monolayer formation of Ag_2O or AgOH.

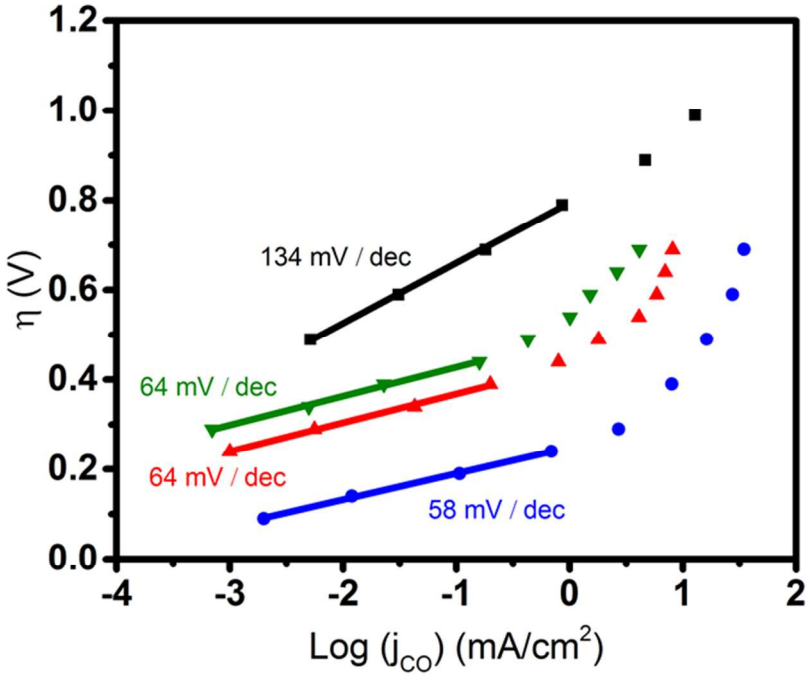

Figure S6: Tafel plots for nanoparticle Ag electrodes with 1 (green) and 10 mg/cm^2 loadings (red). Polycrystalline (black) and nanoporous (blue) Ag catalysts are also shown for comparison.

The 1mg Ag loading results show a similar log-linear region as the 10mg loading data. This indicates that diffusion typically limits CO_2 reduction activity at higher current densities. Attempts to further reduce the Ag loading were not successful due to potentially poor adhesion and/or possibly poor dispersion of nanoparticles over the carbon substrate when an extremely dilute catalyst slurry is used, leading to unreliable data. It is possible that an intermediate region exists where both coverage and diffusion play a role. However, based on the data presented here, the quick increase of overpotential at high currents is very likely due to mass transport rather than coverage effects in the cases of nanostructured Ag.

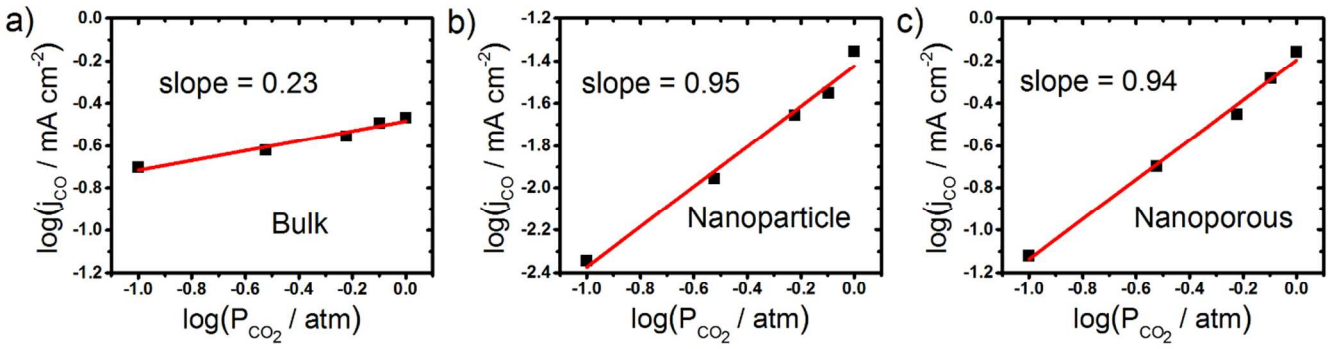

Figure S7: CO_2 partial pressure dependence studies for (a) bulk Ag, (b) nanoparticle Ag, and (c) nanoporous Ag performed at constant potential.

Table S1. pH values of electrolytes used for bicarbonate dependent studies and comparison to electrolyte used for electrocatalyst testing.

$[HCO_3^-]$	$[HClO_4^-]$	pH
0.1	**0.9**	**6.18**
0.2	**0.8**	**6.49**
0.5	**0.5**	**6.95**
0.8	**0.2**	**7.15**
1.0	**0**	**7.41**
0.5	**0**	**7.20**

Table S2. pH values of electrolytes used for partial pressure dependent studies with 0.5M bicarbonate electrolyte.

CO_2 %	N_2 %	pH
10	**90**	**8.41**
30	**70**	**7.90**
60	**140**	**7.56**
80	**20**	**7.40**
100	**0**	**7.20**

Computational methods

Density functional theory (DFT) calculations were performed using the Vienna *ab initio* simulation package (VASP) code,[1–3] with exchange-correlation interactions modeled by the revised Perdew-Burke-Ernzerhof (RPBE) generalized gradient approximation (GGA) functional.[1] Electron-ion interactions were modeled using projector augmented wave (PAW) pseudopotentials.[4,5] All computations were conducted with a plane-wave cutoff of 400 eV and a density cutoff of 650 eV, with 0.1 eV Fermi-level smearing for all surface calculations and 0.01 eV for gas-phase species. Spin-polarization was included in all computations. The flat Ag surfaces, (111) and (100), and the Ag(110) stepped surface were modeled with a 3×3×5 periodic cell. The Ag(211) stepped surface calculations were performed on a 3×3×3 periodic cell, which ensures sufficient depth below edge-adsorbed species. In all cases, the top two layers (plus any adsorbates) were allowed to relax, while the rest of the slab remained fixed. All four periodic cells included at least 15 Å of vacuum, with a Monkhorst-Pack (5,5,1) *k*-point sampling of the Brillouin zone.[6] The convergence criterion was a maximum atomic force of 0.05 eV. For the adsorbates, multiple configurations were considered, and the lowest energy configuration in each case was selected. The lattice constant for Ag used in this study is 4.212 Å, found by optimization of the unit cell with a Monkhorst-Pack (15,15,15) *k*-point sampling.

Gibbs free energies for each gaseous and adsorbed species were calculated at 298.15 K, according to the expression:

$$G = E_{DFT} + E_{ZPE} + \int C_P dT - TS$$

where E_{DFT} is the electronic energy calculated with VASP, E_{ZPE} is the zero-point energy, $\int C_P dT$ is the enthalpic temperature correction, TS is the entropy contribution. Standard ideal gas methods were employed to compute E_{ZPE}, $\int C_P dT$, and TS from temperature, pressure, and calculated vibrational energies.[7] The assumed fugacities reflect approximate product distributions for nanostructured Ag as well as vapor pressure conditions at 298.15 K. For adsorbates, all 3*N* degrees of freedom were treated as frustrated harmonic vibrations with negligible contributions from the Ag surfaces. The calculated values are listed in Table S2.

In the computational hydrogen electrode (CHE) model,[1] each electrochemical reaction step is treated as a simultaneous transfer of the proton-electron pair as a function of the applied potential. Thus, free energy changes relative to an initial state of gaseous CO_2 freely above an empty surface can be represented by

$$\Delta G[COOH^*] = G[COOH^*] - (G[*] + G[CO_2] + G[H^+ + e^-])$$
$$\Delta G[CO^*] = G[CO^*] + G[H_2O] - (G[*] + G[CO_2] + 2 \times G[H^+ + e^-])$$
$$\Delta G[CO] = G[CO] + G[H_2O] - (G[CO_2] + 2 \times G[H^+ + e^-])$$

with

$$G[H^+ + e^-] = \frac{1}{2} G[H_2] - eU$$

where U is the applied overpotential and e is the elementary charge. In this study, $eU = -0.11\ eV$, representing the approximate minimum driving force such that the free energy change of CO_2 to CO is net negative. For all CHE steps, $G[H_2]$ was considered at atmospheric pressure. It should be noted that this method always couples the proton and electron donation; in aqueous systems determination of the true rate-determining step requires the additional experimental analysis outlined in this paper.

In accordance with previous studies, additional energy corrections were applied to produce the final free energy diagrams (Figure 1). As a result of a systematic sensitivity analysis of RPBE gas-phase electronic energies, a +0.45 eV correction was applied to the CO_2 electronic energy.[8] Solvation effects in aqueous solution were treated using a 0.25 eV stabilization of COOH* for all surfaces.[9] Applying these corrections serves to lower the deviation of the DFT values from experiment, but has no impact on the relative energy differences between the Ag surfaces studied here.

As mentioned in the text, additional analysis was performed to examine any formation of adsorbed CO_2 or CO_2^- intermediates, as previously suggested.[9] This analysis was performed by considering multiple possible adsorption sites on Ag (211), (111), (110), and (100) surfaces, followed by relaxation. Within reasonable convergence limits, no stable configuration could be determine for any configuration on any Ag surface, whether or not additional localized charge was included. In the absence of any other direct evidence for a standalone CO_2^- intermediate, we have chosen to represent the initial proton donation, electron transfer, and surface adsorption as simultaneous (Reaction A1).

Table S3: Calculated values for conversion of electronic energies to free energies. Assumed fugacities for gaseous species are also included.

Species/Adsorbate	Fugacity (Pa)	E_{ZPE} (eV)	$\int C_P dT$ (eV)	$-TS$ (eV)	$G - E_{elec}$ (eV)
H_2 (g)	10133	0.269	0.091	-0.462	-0.102
H_2 (1 atm. reference)	101325	0.269	0.091	-0.403	-0.043
CO_2 (g)	101325	0.304	0.099	-0.663	-0.260
CO (g)	91192	0.130	0.091	-0.596	-0.375
H_2O (g)	3173	0.565	0.104	-0.673	-0.004
COOH* on Ag(100)	--	0.574	0.075	-0.152	0.497
CO* on Ag(100)	--	0.152	0.054	-0.109	0.097
H* on Ag(100)	--	0.135	0.019	-0.034	0.120
COOH* on Ag(111)	--	0.577	0.099	-0.224	0.452
CO* on Ag(111)	--	0.145	0.085	-0.220	0.010
H* on Ag(111)	--	0.132	0.009	-0.012	0.129
COOH* on Ag(110)	--	0.580	0.120	-0.279	0.421
CO* on Ag(110)	--	0.147	0.058	-0.128	0.077
H* on Ag(110)	--	0.131	0.010	-0.013	0.128
COOH* on Ag(211)	--	0.587	0.116	-0.257	0.446
CO* on Ag(211)	--	0.153	0.053	-0.105	0.101
H* on Ag(211)	--	0.141	0.014	-0.022	0.133

Expanded derivation of the nanostructured Ag mechanism

While the critical results of the Tafel analysis and reaction order analysis are presented in the main text, we here provide a more stepwise approach to deriving these quantities. Beginning with reaction mechanism outlined in Equations A1-A3 and taking Equation A2-1 as the rate-determining step, we start by writing the rate expression as a function of coverage:

$$i_{CO} = nFk_{\mathrm{A2-1}}\theta_{COOH}[H_2O]$$

If we assume that the first step in the mechanism is in fast equilibrium, then we can write:

$$k_{\mathrm{A1}}P_{CO_2}[HCO_3^-](1-\theta)\exp\left(\frac{-\beta_{A1}EF}{RT}\right) = k_{-\mathrm{A1}}[CO_3^{2-}]\theta_{COOH}\exp\left(\frac{(1-\beta_{A1})EF}{RT}\right)$$

$$\frac{\theta_{COOH}}{(1-\theta)} = \mathrm{K}_1\, exp\left(\frac{-EF}{RT}\right)\frac{\mathrm{P}_{\mathrm{CO}_2}[\mathrm{HCO}_3^-]}{[\mathrm{CO}_3^{2-}]}$$

Assuming θ (the overall coverage) is small yields Equation 3, as shown in the main text:

$$\mathrm{i}_{CO} = nF\mathrm{K}_1k_2\exp\left(\frac{-EF}{RT}\right)P_{CO_2}\frac{[HCO_3^-][H_2O]}{[CO_3^{2-}]}$$

However for the partial pressure and bicarbonate concentration study, Equation 3 in the main text can instead be expressed for a constant-overpotential measurement. This is crucial due to the pH dependence of the electrolyte as a function of the partial pressure of P_{CO_2} and $[HCO_3^-]$. To show the reaction order with respect to these variables, we first take the log of both sides of Equation 3 to obtain:

$$\log(i_{CO}) = \log\left(nFK_{\mathrm{A1}}k_{\mathrm{A2-1}}P_{CO_2}\right) + \frac{-EF}{2.3RT} + \log([HCO_3^-]) + \log\left(\frac{[H_2O]}{[CO_3^{2-}]}\right)$$

The applied potential E is made up of two components: the reversible potential of the reaction and the applied overpotential that we hold constant in these experiments. Substituting in Equation 4 yields:

$$\log(i_{CO}) = \log\left(nFK_{A1}k_{A2-1}P_{CO_2}\right) - \frac{FE^{rev}}{2.3RT} + \frac{F\eta}{2.3RT} + \log([\mathrm{HCO}_3^-]) + \log\left(\frac{[H_2O]}{[CO_3^{2-}]}\right)$$

The reversible potential can be related in terms of the Nernst equation (Equation 5). This expression takes into account an additional factor: changes in chemical potential due to the varying bicarbonate concentration. Thus, we can write:

$$E^{rev} = E^0 - \frac{2.3RT}{2F}\log\left(\frac{[OH^-][CO_3^{2-}]P_{CO}}{P_{CO_2}[HCO_3^-]}\right)$$

based on the overall reaction:

$$CO_2 + HCO_3^- + H_2O + 2e^- \leftrightarrow CO + OH^- + CO_3^{2-} + H_2O$$

With this substitution into the overall rate law, the partial derivative of the CO current density with respect to bicarbonate concentration at constant overpotential will yield an expression for our reaction order equal to 0.5, as shown below:

$$\log(i_{CO}) = \log\left(nFK_{A1}k_{A2-1}P_{CO_2}\right) - \frac{FE^0}{2.3RT} + \frac{1}{2}\log\left(\frac{[OH^-][CO_3^{2-}]P_{CO}}{P_{CO_2}[HCO_3^-]}\right) + \frac{F\eta}{2.3RT} + \log([\mathrm{HCO_3^-}]) + \log\left(\frac{[H_2O]}{[CO_3^{2-}]}\right)$$

$$\log(i_{CO}) = \log\left(nFK_{A1}k_{A2-1}P_{CO_2}\right) - \frac{FE^0}{2.3RT} + \frac{1}{2}\log\left(\frac{[OH^-][CO_3^{2-}]P_{CO}}{P_{CO_2}}\right) + \frac{F\eta}{2.3RT} + \frac{1}{2}\log([\mathrm{HCO_3^-}]) + \log\left(\frac{[H_2O]}{[CO_3^{2-}]}\right)$$

and $\frac{\partial \log(i_{CO})}{\partial [HCO_3^-]} = 0.5$ and $\frac{\partial \log(i_{CO})}{\partial [P_{CO_2}]} = 0.5$

Exclusion of alternate rate determining steps on nanostructured Ag

Here, we examine the effect of other intermediate coverages on the Tafel slope and other reactant dependencies to further confirm our proposed mechanism. We also present a thorough analysis of other potential rate-determining steps to demonstrate that the expected Tafel slopes and reaction orders with respect to P_{CO_2} and HCO_3^- would not be consistent with our experimental observations, further confirming our proposed mechanism

Given our proposed mechanism as re-written below, we can derive the expected Tafel slopes as a function of each reaction intermediate for each of the possible rate-determining steps (overall results from this analysis are shown in Table 1 of the main text):

(A1) $CO_2 + HCO_3^- + e^- + * \rightarrow COOH_{ads} + CO_3^{2-}$
(A2-1) $COOH_{ads} + H_2O \rightarrow COOH_{ads} \cdots H^+ + OH^-$
(A2-2) $COOH_{ads} \cdots H^+ + e^- \rightarrow CO_{ads} + H_2O$
(A3) $CO_{ads} \rightarrow CO + *$

With the exception of the rate-determining step, we assume all other steps are in quasi-equilibrium as given by the following expressions (note that the coverage of $COOH_{ads} \cdots H^+$, the reactive intermediate from step A2-1 preceding electron transfer in step A2-2, is written as θ_{C-H} for simplicity):

$$K_{A1} = \frac{\theta_{COOH}[CO_3^{2-}]}{P_{CO_2}[HCO_3^-]\theta^*} \quad K_{A2-1} = \frac{\theta_{C-H}[OH^-]}{\theta_{COOH}[H_2O]} \quad K_{A2-2} = \frac{\theta_{CO}[H_2O]}{\theta_{C-H}} \quad K_{A3} = \frac{P_{CO}\theta^*}{\theta_{CO}}$$

Each K_i is an electrochemical equilibrium constant as defined by:

$$K_i = \exp\left(\frac{-\Delta G_{i,0} - n_i F\left(E - E_i^0\right)}{RT}\right)$$

In steps A2-1 and A3 there is no electron transfer, and so $n_{A2-1,A3} = 0$. For steps A1 and A2-2, $n_{A1,A2-2} = 1$. For each possible case of the rate-determining step, the forward electrochemical rate constant is defined as:

$$k_i = k_i^0 \exp\left(\frac{-\Delta G_{i,0} - n_i \beta_i F\left(E - E_i^0\right)}{RT}\right)$$

In all cases, we define the Tafel slope for a given rate expression as:

$$\text{slope} = -\frac{2.3}{\frac{\delta \ln i}{\delta E}}$$

In the main text, we assert that step A2-1 is the rate-determining step on nanostructured Ag, so we first show the expected Tafel slope for the overall rate expression:

$$i_{CO} = k_{A2-1}\theta_{COOH}[H_2O]$$

With the remaining steps in quasi-equilibrium, we can then write:

$$\theta_{CO} = \frac{P_{CO}\theta^*}{K_{A3}}$$
$$\theta_{C-H} = \frac{\theta_{CO}[H_2O]}{K_{A2-2}} = \frac{P_{CO}\theta^*[H_2O]}{K_{A2-2}K_{A3}}$$
$$\theta_{COOH} = \frac{P_{CO_2}[HCO_3^-]\theta^*}{[CO_3^{2-}]}K_{A1}$$

Then, the overall rate concentration of open surface sites may be written as:

$$\theta^* = \frac{1}{1 + \frac{P_{CO_2}[HCO_3^-]}{[CO_3^{2-}]}K_{A1} + \frac{P_{CO}[H_2O]}{K_{A2-2}K_{A3}} + \frac{P_{CO}}{K_{A3}}}$$

By substitution of these expressions into the rate equation and taking the derivative with respect to the potential, E, the slope is found to be:

Tafel slope, 2nd step RDS (A2-1) = $\frac{2.3RT}{F(1-\theta_{COOH}+\theta_{C-H})}$

For illustrative purposes, the complete derivation of this expression is as follows:

$$\ln i = \ln k_{A2-1} + \ln\theta_{COOH} + \ln[H_2O]$$
$$= \ln k_{A2-1} + \ln[H_2O] + \ln\theta^* + \ln K_{A1} + \ln\left(\frac{P_{CO_2}[HCO_3^-]}{[CO_3^{2-}]}\right)$$

$$\frac{\delta \ln i}{\delta E} = \frac{\delta}{\delta E}\left(\ln k_{A2-1} + \ln[H_2O] + \ln\theta^* + \ln K_{A1} + \ln\left(\frac{P_{CO_2}[HCO_3^-]}{[CO_3^{2-}]}\right)\right) = \frac{\delta}{\delta E}(\ln K_{A1} + \ln\theta^*)$$

$$= -\frac{F}{RT} + \frac{\delta}{\delta E}\ln\theta^* = -\frac{F}{RT} - \frac{\delta}{\delta E}\ln\frac{1}{\theta^*} = -\frac{F}{RT} - \theta^*\frac{\delta\left(\frac{1}{\theta^*}\right)}{\delta E}$$

$$\frac{\delta \ln i}{\delta E} = -\frac{F}{RT} - \theta^*\frac{\delta}{\delta E}\left(1 + \frac{P_{CO_2}[HCO_3^-]}{[CO_3^{2-}]}K_{A1} + \frac{P_{CO}[H_2O]}{K_{A2-2}K_{A3}} + \frac{P_{CO}}{K_{A3}}\right)$$

$$= -\frac{F}{RT} - \theta^*\left(\frac{F}{RT}\right)\left(-\frac{P_{CO_2}[HCO_3^-]}{[CO_3^{2-}]}K_{A1} + \frac{P_{CO}[H_2O]}{K_{A2-2}K_{A3}}\right)$$

$$= -\frac{F}{RT}(1 - \theta_{COOH} + \theta_{C-H})$$

$$\text{slope} = \frac{2.3}{-\frac{\delta \ln i}{\delta E}} = \frac{2.3RT}{F(1 - \theta_{COOH} + \theta_{C-H})}$$

In general, we assume that the $COOH_{ads} \cdots H^+$ intermediate is very short-lived, with $\theta_{C-H} \ll 1$. As derived, the Tafel slope should then be 59 mV dec^{-1} at $\theta_{COOH} \ll 1$, which we assume to be true in the kinetically-limited, low-current regime on nanostructured Ag. This low-current regime is further supported by order and linearity of the P_{CO_2} and $[HCO_3^-]$ dependence studies, as shown in the main text. The form of this Tafel slope expression also supports our observations on bulk, with an expected Tafel slope of 118 mV dec^{-1} at $\theta_{COOH} = 0.5$.

If we assume instead that the 1st step, A1, is rate-determining, then:

$$i_{CO} = k_{A1}P_{CO_2}[HCO_3^-]\theta^*$$

$$\theta_{CO} = \frac{P_{CO}\theta^*}{K_{A3}}$$

$$\theta_{C-H} = \frac{\theta_{CO}[H_2O]}{K_{A2-2}} = \frac{\theta^* P_{CO}[H_2O]}{K_{A2-2}K_{A3}}$$

$$\theta_{COOH} = \frac{\theta_{C-H}[OH^-]}{[H_2O]K_2} = \frac{P_{CO}\theta^*[OH^-]}{K_{A2-1}K_{A2-2}K_{A3}}$$

$$\theta^* = \frac{1}{1 + \frac{P_{CO}[OH^-]}{K_{A2-1}K_{A2-2}K_{A3}} + \frac{P_{CO}[H_2O]}{K_{A2-2}K_{A3}} + \frac{P_{CO}}{K_{A3}}}$$

Tafel slope, 1st step RDS (A1) = $\frac{2.3RT}{F(\beta_{A1} + \theta_{COOH} + \theta_{C-H})}$

In this case, we can see that the Tafel slope at low coverage of all intermediates would be 118 mV dec^{-1}, assuming $\beta_{A1} = 0.5$. With increasing θ_{COOH}, the Tafel slope would be expected to *decrease*: first to 59 mV dec^{-1} at $\theta_{COOH} = 0.5$, then down to 39 mV dec^{-1} at $\theta_{COOH} = 1$. We find this behavior to be counterintuitive, and the necessity of moderate to high coverage to match our observed Tafel slope on nanostructured Ag does not agree with our reaction order studies for P_{CO_2} and $[HCO_3^-]$.

If the 3rd step, A2-2 is rate-determining, then:

$$i_{CO} = k_{A2-2}\theta_{C-H}$$

$$\theta_{CO} = \frac{P_{CO}\theta^*}{K_{A3}}$$

$$\theta_{C-H} = \frac{\theta_{COOH}[H_2O]}{[OH^-]}K_{A2-1} = \frac{\theta^* P_{CO_2}[HCO_3^-][H_2O]}{[CO_3^{2-}][OH^-]}K_{A1}K_{A2-1}$$

$$\theta_{COOH} = \frac{P_{CO_2}[HCO_3^-]\theta^*}{[CO_3^{2-}]}K_{A1}$$

$$\theta^* = \frac{1}{1+\frac{P_{CO_2}[HCO_3^-]}{[CO_3^{2-}]}K_{A1}+\frac{P_{CO_2}[HCO_3^-][H_2O]}{[CO_3^{2-}][OH^-]}K_{A1}K_{A2-1}+\frac{P_{CO}}{K_{A3}}}$$

Tafel slope, 3rd step RDS (A2-2) = $\frac{2.3RT}{F(\beta_{A2-2}+1-\theta_{COOH}-\theta_{C-H})}$

If $\beta_{A2-2} = 0.5$, then at maximum coverage the Tafel slope would be 118 mV dec^{-1}. At low coverage, however, the expected value is 39 mV dec^{-1}, which is considerably lower than the value we observe at low overpotentials on nanostructured Ag. For this to be the correct rate-determining step, then we would need to be operating at intermediate coverage of θ_{COOH} to obtain our observed Tafel slope of 59 mV dec^{-1}. In that region, however, there would be a non-linear response for the P_{CO_2} and $[HCO_3^-]$ dependence studies, as well as lower expected values than those observed in Figure 3.

It also follows that the combination of A2-1 and A2-2 as a single rate-determining step would result in a slope of:

Tafel slope, 2nd and 3rd step combined as RDS (A2) = $\frac{2.3RT}{F(\beta_{A2-2}+1-\theta_{COOH})}$

Given anticipated low coverages of $COOH_{ads} \cdots H^+$, the result is effectively the same as that obtained for A2-2 as the rate-determining step. Therefore, we maintain that A2-1, decoupled from A2-2, is most likely the rate-determining step on nanostructured Ag.

Finally, if the 4th step, A3, were rate-determining, then the following is the derivation of the Tafel slope:

$$i_{CO} = k_{A3}\theta_{CO}$$

$$\theta_{CO} = \frac{\theta_{C-H}}{[H_2O]}K_{A2-2} = \frac{\theta^* P_{CO_2}[HCO_3^-]}{[OH^-][CO_3^{2-}]}K_{A1}K_{A2-1}K_{A2-2}$$

$$\theta_{C-H} = \frac{\theta_{COOH}[H_2O]}{[OH^-]}K_{A2-1} = \frac{\theta^* P_{CO_2}[HCO_3^-][H_2O]}{[OH^-][CO_3^{2-}]}K_{A1}K_{A2-1}$$

$$\theta_{COOH} = \frac{P_{CO_2}[HCO_3^-]\theta^*}{[CO_3^{2-}]}K_{A1}$$

$$\theta^* = \frac{1}{1+\frac{P_{CO_2}[HCO_3^-]}{[CO_3^{2-}]}K_{A1}+\frac{P_{CO_2}[HCO_3^-][H_2O]}{[OH^-][CO_3^{2-}]}K_{A1}K_{A2-1}+\frac{P_{CO_2}[HCO_3^-]}{[OH^-][CO_3^{2-}]}K_{A1}K_{A2-1}K_{A2-2}}$$

Tafel slope, 4th step RDS (A3) = $\frac{2.3RT}{F(2-\theta_{COOH}-\theta_{C-H}-2\theta_{CO})}$

Notably, this is the only choice of the rate-determining step which results in an explicit dependence on θ_{CO}. While it remains reasonable to assume that a $COOH_{ads} \cdots H^+$ species would be short-lived, both θ_{COOH} and θ_{CO} could plausibly be greater than zero. However, CO does not strongly adsorb on Ag and falls in a region of CO binding strength where $CO_{(g)}$ is greatly favored over CO_{ads}, with an adsorption energy of CO more than 0.3 eV weaker than Au.[10] Therefore, as in the case of Au operating at low overpotentials, we expect to see negligible θ_{CO} on Ag in the Tafel regime and do not expect that desorption would be rate-limiting.[11] In the region of low overall coverage, the expected Tafel slope for this case is 30 mV dec^{-1}, which is not supported by our measurements at low overpotential.

Determination of the Proton Donor Sources and Justification for Coupling Reactions

In the text, we suggest that the first proton transfer occurs from HCO_3^- (and cannot be decoupled from the electron transfer), while the second proton transfer occurs from H_2O, H^+ or other adsorbed H and is followed by an electron transfer (Equations A1-A3, including A2-1 and A2-2). As presented in the main text (Equation 5), the Nernst equation for the overall reaction $CO_2 + HCO_3^- + H_2O + 2e^- \leftrightarrow CO + OH^- + CO_3^{2-} + H_2O$ can be expressed as:

$$E^{rev} = E^0 - \frac{2.3RT}{2F}\log\left(\frac{[OH^-][CO_3^{2-}]P_{CO}}{P_{CO_2}[HCO_3^-]}\right) \qquad \text{(NE1)}$$

If the order of proton donors were reversed, then the Nernst equation would remain the same as NE1, since the overall reaction is maintained. For the nanostructured Ag surface, the overall rate expression at low coverage could then be expressed as

$$i_{CO} = nFk_2K_1 \exp\left(\frac{-EF}{RT}\right) P_{CO_2} \frac{[HCO_3^-][H_2O]}{[OH^-]} \qquad \text{(REN1)}$$

which produces an expected reaction order of 1 for P_{CO_2} at constant potential, as well as a Tafel slope of 59 mV dec^{-1} that remains consistent with our experimental observations. It also appears that the reaction order is 0.5 for $[HCO_3^-]$ at constant overpotential. Though we are inclined to still assume that HCO_3^- would not easily protonate species adsorbed to the negatively-charged surface, there is no inconsistency in the derived rate expressions are apparent reaction orders caused by swapping the order of proton donors.

If both proton donors were HCO_3^-, then the overall reaction would change to $CO_2 + 2HCO_3^- + 2e^- \leftrightarrow CO + 2CO_3^{2-} + H_2O$ and the Nernst equation would be:

$$E^{rev} = E^0 - \frac{2.3RT}{2F}\log\left(\frac{[H_2O][CO_3^{2-}]^2 P_{CO}}{P_{CO_2}[HCO_3^-]^2}\right) \qquad \text{(NE2)}$$

For nanostructured Ag, the rate expression becomes

$$i_{CO} = nFk_2K_1 \exp\left(\frac{-EF}{RT}\right) P_{CO_2} \frac{[HCO_3^-]^2}{[CO_3^{2-}]} \quad \text{(REN2)}$$

It follows that the reaction order with respect to $[HCO_3^-]$ at constant overpotential would be 1, which is again inconsistent with experimental evidence.

In the case of H_2O as the sole proton donor, the overall reaction becomes $CO_2 + 2H_2O + 2e^- \leftrightarrow CO + 2OH^- + H_2O$ and the Nernst equation could be expressed as:

$$E^{rev} = E^0 - \frac{2.3RT}{2F} \log\left(\frac{[OH^-]^2 P_{CO}}{P_{CO_2}[H_2O]}\right) \quad \text{(NE3)}$$

While we obtain the expected values for the Tafel slope and P_{CO_2} dependence, there would be no explicit inclusion of $[HCO_3^-]$ on either surface. Thus, we do not expect both proton sources to derive from water.

Finally, there is the case where the second proton and electron transfer is not decoupled over nanostructured Ag. In this case, we would expect the rate expression to be

$$i_{CO} = nFk_2K_1 \exp\left(\frac{-(1+\beta)EF}{RT}\right) P_{CO_2} \frac{[HCO_3^-][H_2O]}{[CO_3^{2-}]} \quad \text{(REN3)}$$

This expression yields a Tafel slope of approximately 40 mV dec^{-1} (though all reaction orders are the same as previous results). Given our experimental evidence, we find that the second proton transfer must occur before the second electron transfer.

Table S4: Summary of Alternate Reaction Schemes

Scheme	Nernst equation	Tafel Slope (mV/dec.)	Order wrt. P_{CO_2} C.P.	Order wrt. $[HCO_3^-]$ C.O.
First proton donor [$\boldsymbol{H_2O}$] and second proton donor [$\boldsymbol{HCO_3^-}$]	NE1	59	1	0.5
Both donors [HCO_3^-]	NE2	59	1	**1**
Both donors [H_2O]	NE3	59	1	**n/a**
Second proton/electron transfer not decoupled	NE1	**39**	1	0.5

Note: C.P. denotes "at constant potential", while C.O. denotes "at constant overpotential. Text in red denotes values that do not agree with our experimental evidence.

References:

(1) Hammer, B.; Hansen, L.; Nørskov, J. *Phys. Rev. B*, 1999, *59*, 7413–7421.

(2) Kresse, G. *Phys. Rev. B*, 1996, *54*, 11169–11186.

(3) Kresse, G.; Furthmüller, J. *Comput. Mater. Sci.* **1996**, *6*, 15–50.

(4) Blöchl, P. E. *Phys. Rev. B* **1994**, *50*, 17953–17979.

(5) Kresse, G. *Phys. Rev. B*, 1999, *59*, 1758–1775.

(6) Monkhorst, H.; Pack, J. *Phys. Rev. B* **1976**, *13*, 5188–5192.

(7) Cramer, C. J. *Essentials of Computational Chemistry Theories and Models*; 2004; Vol. 42, pp. 334–342.

(8) Tripkovic, V.; Skulason, E.; Siahrostami, S.; Norskov, J. K.; Rossmeisl, J. *Electrochim. Acta* **2010**, *55*, 7975–7981.

(9) Hori, Y. In *Modern Aspects of Electrochemistry*; 2008; Vol. 42, pp. 89–189.

(10) Kuhl, K. P.; Hatsukade, T.; Cave, E. R.; Abram, D. N.; Kibsgaard, J.; Jaramillo, T. F. *J. Am. Chem. Soc.* **2014**, *136*, 14107–14113.

(11) Akhade, S. A.; Luo, W.; Nie, X.; Bernstein, N. J.; Asthagiri, A.; Janik, M. J. *Phys. Chem. Chem. Phys.* **2014**, *16*, 20429–20435.